SCIENTIFIC REPORTS

OPEN

SUBJECT AREAS:
DNA DAMAGE RESPONSE
ORAL CANCER
RADIOTHERAPY

Received
5 November 2013

Accepted
19 May 2014

Published
6 June 2014

Correspondence and requests for materials should be addressed to K.H.L. (limesank@u.arizona.edu) or D.K.A. (dann@coh.org)

Autophagy Correlates with Maintenance of Salivary Gland Function Following Radiation

Maria Morgan-Bathke[1], Grace A. Hill[1], Zoey I. Harris[1], Her H. Lin[4], Alex M. Chibly[2], Rob R. Klein[3], Randy Burd[1], David K. Ann[4] & Kirsten H. Limesand[1]

[1]Department of Nutritional Sciences, University of Arizona, Tucson, AZ 85721, USA, [2]Cancer Biology Graduate Interdisciplinary Program, University of Arizona, Tucson, AZ 85721, USA, [3]Department of Pathology, University of Arizona, Tucson, AZ 85721, USA, [4]Department of Molecular Pharmacology, Beckman Research Institute, City of Hope Medical Center, Duarte, CA 91010, USA.

The current standard of care for head and neck cancer includes surgical resection of the tumor followed by targeted head and neck radiation. This radiotherapy results in a multitude of negative side effects in adjacent normal tissues. Autophagy is a cellular mechanism that could be targeted to ameliorate these side effects based on its role in cellular homeostasis. In this study, we utilized *Atg5*$^{f/f}$*;Aqp5-Cre* mice which harbor a conditional knockout of *Atg5*, in salivary acinar cells. These autophagy-deficient mice display increased radiosensitivity. Treatment of wild-type mice with radiation did not robustly induce autophagy following radiotherapy, however, using a model of preserved salivary gland function by IGF-1-treatment prior to irradiation, we demonstrate increased autophagosome formation 6–8 hours following radiation. Additionally, administration of IGF-1 to *Atg5*$^{f/f}$*;Aqp5-Cre* mice did not preserve physiological function. Thus, autophagy appears to play a beneficial role in salivary glands following radiation and pharmacological induction of autophagy could alleviate the negative side effects associated with therapy for head and neck cancer.

Head and neck cancer is one of the most common cancers worldwide. The current standard of care includes surgical resection of the tumor followed by chemotherapy and radiation[1]. Although advances in technology have allowed for improved targeting of radiation to the tumor, salivary glands still receive significant levels of radiation throughout the course of treatment[2]. Radiation causes significant damage to the salivary glands and a loss of salivary function. This damage causes patients to suffer from xerostomia, mucositis, dental caries and malnutrition[2,3]. Unfortunately, current therapies used to ameliorate these negative side effects are short-lived and have multiple negative side effects of their own[2,3]. Therefore, it is consequential that mechanisms for salivary gland preservation be identified to better the quality of life for these patients and decrease their financial burden.

Macroautophagy, hereafter referred to as autophagy, has been shown to have both positive and negative effects on cellular homeostasis and survival[4,5]. In a majority of tissues, autophagy is necessary to maintain cellular homeostasis and to provide a "quality control" mechanism via removal of damaged proteins and organelles[4,5]. The role of autophagy in the response of cancer cells to radiotherapy has been studied in depth[6–12]; however, the role autophagy plays in normal tissue function following radiation is much less understood. When a knockdown of Atg7 was used in human prostatic epithelial cell line, RWPE-1, these cells showed increased radiosensitivity and increased non-apoptotic cell death[13]. However, Moretti *et al* found that the induction of autophagy in mouse embryonic fibroblasts (MEFs) following radiation actually increased radiosensitivity via increased levels of non-apoptotic cell death[14]. Therefore the beneficial or detrimental effect by autophagy may be cell type- and damage stimulus-dependent and much more research is needed to define the role of autophagy in physiologic function following damage.

Mouse models have been extensively used to investigate the mechanisms underlying salivary gland sensitivity to radiation-therapy. These studies have shown that there is a significant increase in apoptosis of salivary acinar cells 8–24 hours following targeted head and neck radiation[15]. This increase in cell death is most likely one of the causes of the loss of acinar cells, glandular shrinkage, changes in saliva composition, and reduction in salivary flow rates which occurs within 72 hours after radiation[2]. In addition, there is a lack of cell cycle arrest in the salivary glands at these acute time points following radiation[16]. It is hypothesized that this lack of cell cycle arrest does not allow sufficient time for cells to undergo repair following radiotherapy. Models of preventing radiation-induced

salivary gland dysfunction have primarily focused on regulation of apoptosis. The use of insulin like growth factor-1 (IGF-1) concurrently with targeted head and neck radiation causes a significant reduction in the rate of apoptosis and increased cell cycle arrest at these acute time points[17]. Importantly, radiation with IGF-1 pretreatment also allows for preservation of stimulated salivary flow rates[17–19].

The activation of autophagy in normal tissue following stress, such as radiation, may rely in part on the interplay between apoptosis and autophagy. The exact relationship between these two cellular mechanisms remains controversial and is most likely tissue and stress specific[19]. Most studies, however, do describe Ambra1, Beclin-1, and Bcl-2 as key proteins in the interplay between these two cellular processes[17–20]. Ambra1 and Beclin-1 are necessary for the autophagic process to occur. These two proteins form a complex that is required for the second step of the autophagic process, elongation of the phagophore[21]. Bcl-2 sequesters Ambra1 so that it is unable to complex with Beclin-1 and leads to an inhibition of autophagy and an induction of apoptosis[17,20]. Therefore, studying the interaction and crosstalk relationship of these three proteins can help expand the understanding of the autophagy/apoptosis relationship.

We created the *Atg5$^{f/f}$;Aqp5-Cre* mouse model which has a conditional knockout of *Atg5*, a gene necessary for autophagy, in salivary acinar cells in order to understand the role of autophagy in salivary gland function[22]. In these mice, *Cre* recombinase is specifically expressed in salivary acinar cells via the use of the Aquaporin 5 (Aqp5) promoter, which is the principle aquaporin water channel protein expressed on the apical surface of salivary acinar cells[23]. Salivary glands have relatively low baseline levels of autophagy[24] and correspondingly *Atg5$^{f/f}$;Aqp5-Cre* mice display no differences in baseline levels of apoptosis, proliferation, or salivary flow rates[22]. The purpose of this study was to determine the role of autophagy in the response of the salivary glands to targeted head and neck radiation and to better define the relationship between autophagy and apoptosis in salivary glands following radiation by evaluating the binding of Ambra-1 to Bcl-2 or Beclin-1.

Methods

Ethics statement. All animals were housed and treated in accordance with the University of Arizona Institutional Animal Care and Use Committee (IACUC). All experiments were approved by IACUC.

Production of *Atg5$^{f/f}$;Aqp5-Cre* mice. The development of the *Atg5$^{f/f}$;Aqp5-Cre* mice has been described in detail previously[22]. Briefly, an *Aqp5-Cre* mouse line was crossed with a mouse line that contains a floxed *Atg5* gene (*Atg5$^{f/f}$*) to produce the *Atg5$^{f/f}$;Aqp5-Cre* autophagy-deficient and *Atg5$^{+/+}$;Aqp5-Cre* wild-type mice. DNA was isolated from tail tips to determine the genotype of each mouse. 2 μl of *Atg5* or *Cre* recombinase primer pairs (IDT) and 1 μl of isolated DNA were added to Hot Start PCR Mix Tubes (Bioneer, Alameda, CA). The Hot Start PCR Mix Tubes were placed into a thermal cycler for 2 hours (Bio-Rad). This PCR mixture was loaded into an agarose gel with ethidium bromide and run at 150 volts for about 30 minutes. The VersaDoc Imaging System (Bio-Rad) was used to image the ethidium bromide gels. Both male and female mice were used for all experiments using this mouse model.

Radiation treatment. Intramuscular injections of a ketamine/xylazine mixture (50 mg/kg and 10 mg/ml respectively) (Western Medical Supply, Arcadia, CA) were given to four to six week old FVB, *Atg5$^{f/f}$;Aqp5-Cre*, or *Atg5$^{+/+}$;Aqp5-Cre* mice for sedation. Following sedation, the mice were constrained in a 50 ml conical tube and their bodies were shielded with >6 mm lead so that only the head and neck region was exposed to a single 5 Gy dose of radiation (^{60}Co therapeutic irradiator, Theratron-80, Atomic Energy of Canada Ltd., Ottawa, Canada). All animals were housed and treated in accordance with the University of Arizona Institutional Animal Care and Use Committee (IACUC). Both male and female mice were used for radiation experiments. Radiation was administered between 8–10am.

Saliva collection and composition. Mice were injected intraperitoneally (i.p.) with carbachol (0.25 mg/kg body weight) and whole saliva was then collected from each mouse for 5 minutes immediately following the injection. Whole saliva was collected into pre-weighed tubes and immediately placed on ice. Salivary flow rates were normalized to the average of the untreated group for each treatment group, for each collection day as previously described[25]. Total protein composition of saliva was determined using the Bio-Rad Experion System. Samples were treated and analyzed for amylase concentration according to the Experion Pro260 Analysis Kit protocol. Both male and female mice were used for saliva collection experiments. Saliva collections were always completed in the morning.

Histology. Salivary gland tissue was removed and immediately fixed in 10% formalin (Fisher Scientific) for 24 hours and next placed into 70% ethanol. Tissues were paraffin embedded, serial sectioned (4 μm) by the Histology Service Laboratory in the Department of Cellular and Molecular Medicine at the University of Arizona. Both male and female mice were used for histology experiments.

Amylase area staining. Serial sectioned slides, as described above, were baked for 45 minutes at 37°C. Slides were then rehydrated in Histoclear, 100% ethanol, 95% ethanol, 70% ethanol, 50% ethanol and water for 10 minutes each. Slides were then placed in citric acid (0.01 M) and microwaved for 10 minutes. The slides were left in the 0.01 M citric acid for 20 minutes at room temperature. After this incubation, slides were washed in PBS for 15 minutes and the tissues were then outlined using a wax pen. 0.5% NEN was used to block slides at room temperature for 1 hour and they were then incubated in a 1 : 500 dilution anti-amylase primary antibody (Sigma Aldrich St. Loius, MO) overnight at 4°C. Slides were then washed with PBS and incubated in anti-rabbit Cy2-conjugated secondary antibody (1 : 500) (Invitrogen Grand Island, NY) at room temperature for 1 hour. Next the slides were counterstained with DAPI and mounted with 50% glycerol in 10 mM Tris-HCl. Fluorescent images were visualized on a Leica DM5500 Microscope System and digitally captured with a Pursuit 4 Megapixel CCD camera using Image Pro 7.0 software and morphometric analysis was performed with ImagePro 7.0 (Media Cybernetics Rockville, MD). Twenty fields of view (FOV = 0.39 mm^2) were used to determine positive amylase area. Amylase area is expressed as the percentage of tissue area stained positive for amylase to the total area of the parotid gland and the threshold fluorescence range was equivalent for all slides imaged.

Western blotting. Parotid glands were dissected and homogenized in RIPA buffer with 5 mM sodium orthovanadate (Fisher Scientific, Waltham, MA), protease inhibitor cocktail (Sigma-Aldrich, St. Louis, MO) and 100 mM PMSF (Pierce/Thermo Scientific, Rockford, IL). The samples were then boiled for 10 minutes and sonicated until homogenous. 12% polyacrylamide gels were used and 100 mg of each protein sample was added to the gel. The gels were then transferred to 0.45 μm Immobilon-P membranes (Millipore, Billerica, MA). The membranes were blocked using either non-fat dry milk or 5% BSA and then immunoblotted with one of the following antibodies: anti-β-Tubulin (Thermo Scientific, Waltham, MA), anti-Atg5 (Novus Biologicals, Littleton, CO), anti-Atg7 (Cell Signaling, Boston, MA), anti-LC3 (Nanotools, Teningen, Germany), anti-Ambra1 (Cell Signaling), anti-Beclin-1 (Cell Signaling), anti-Bcl-2 (Cell Signaling). For detection, ECL substrate (Pierce/Thermo Scientific) was used as instructed by the manufacturer. Restore Western Blotting Stripping buffer (Fisher Scientific) was used to strip membranes and then they were blocked and re-probed as described above. All images are cropped for display to allow for clarity in the manuscript. All important bands are included in the cropped images.

Densitometry. Black and white images of Western membranes were imported into Image J software for quantification of bands as per the Image J Software Guide[26]. Quantified bands from 2–3 animals per treatment group and time point were then normalized to their loading control (Tubulin) and displayed as a ratio to the loading control.

Immunohistochemical staining for Atg5 and LC3. Serial sectioned slides as described above were stained utilizing Atg5 or LC3 antibodies to determine levels of autophagy. Slides were dehydrated and antigen retrieval was performed as described for amylase area staining above. Slides were blocked using the ABC Rabbit Kit (Vector Laboratories Burlingame, CA) for 20 minutes and then incubated in their respective primary antibody at 4° C overnight. The next day slides were washed in PBS three times for 10 minutes each and then washed in hydrogen peroxide (1%) for 5 minutes. Slides were again washed in PBS two times for 5 minutes each and then incubated in biotinylated secondary antibody (ABC Rabbit Kit, Vector Laboratories) for 50 minutes at room temperature. Following incubation, slides were washed in PBS three times for 5 minutes each and incubated in ABC reaction kit (Vector Laboratories) for 30 minutes. Then, slides were washed in PBS three times for 5 minutes each and incubated in 3, 3′ Diaminobenzidine[27] for 6 minutes. The slides were washed in water to stop the DAB reaction and stained in hematoxylin for about 2 seconds. Next, slides were rinsed with water for 10 minutes. Slides were dehydrated in 50% ethanol, 70% ethanol, 95% ethanol, 100% ethanol, and Histoclear for 10 minutes each. Coverslips were mounted over the tissue using Permount (Fisher Scientific). The stained tissue sections were visualized using light microscopy and images were taken with a Leica DM5500 (Leica Microsystems, Wetzlar, Germany) and a 4-megapixel Pursuit camera (Diagnostic Instruments, Inc, Sterling Heights, MI).

Transmission electronic microscopy (TEM). Salivary glands were dissected and prepared for imaging as previously described[28]. Samples were viewed using a FEI Tecnai 12 TEM equipped with a Gatan Ultrascan 2K CCD camera. The number of autophagosomes and lysosomes (Ly) were counted from randomly selected regions and normalized to tissue area (100 μm^2).

IGF-1 injections. Following sedation as described above, mice received an intravenous injection of recombinant human IGF-1 (5 μg GroPrep, Adelaide, Australia) immediately prior to targeted head and neck radiation.

Quantification of activated caspase-3 levels. Serial sectioned slides as described above were stained for activated caspase-3 as a marker for apoptosis. Staining procedures were performed as described above and visualized using light microscopy. Images were taken with a Leica DM5500 and a 4-megapixel Pursuit camera. Activated caspase-3 positive acinar cells were quantified by averaging the number of positive cells/total number of cells from five fields of view/mouse.

Immunoprecipitation. Parotid glands were excised and protein was isolated as described above. A Direct IP Kit (Thermo Fisher Scientific) was then used per the manufacturer's specifications. Briefly, 1 mg of protein lysate was added to a spin column containing an Agarose Resin slurry (provided in IP Kit) and incubated at 4°C for one hour. Anti-Ambra1 (Cell Signaling) was then added and incubated at 4°C overnight. On the second day, the antibody/lysate solution was added to a spin column containing Protein A/G agarose (provided in IP Kit). The spin column and antibody/lysate were then washed with a Lysis Wash Buffer and Conditioning Buffer (provided in IP Kit). Next, a sample buffer elution was prepared using 5× Lane Reducing Buffer (provided in IP Kit), dithiothreitol (DTT), and deionized water. This sample buffer elution was added to the antibody/lysate solution and then loaded into a 12% SDS-PAGE gel and run overnight as described above. The membranes were blocked using 5% BSA and then immunoblotted with Ambra1, Beclin-1, and Bcl-2.

Statistical analysis. All statistical analyses were conducted using a one-way analysis of variance (ANOVA) followed by a Bonferroni post-hoc test. To perform the statistical analyses the InStat GraphPad 3 (San Diego, CA) software was used. Salivary flow rates were standardized to untreated groups before the statistical analysis was performed. Groups with the same letter are not statistically different from one another.

Results

Targeted head and neck radiation significantly decreases stimulated salivary flow rates in conditional autophagy-deficient Atg5$^{f/f}$;Aqp5-Cre mice when compared to Atg5$^{+/+}$;Aqp5-Cre mice. Our lab uses a single 5 Gy dose of radiation as this dose allows for physiologically, molecular, and histological changes. Importantly, the clinical fraction of radiation used on patients is 2 Gy/day. Clinically salivary glands display a loss of function acutely following radiation (within the 1st week), therefore it is critically imperative to understand the mechanisms behind lower doses of radiation[29]. There are very few studies on the role of autophagy in the function of non-cancerous tissues following radiation[30–32]. We determined if loss of autophagy was able to alter radiosensitivity of salivary glands following targeted head and neck radiation by utilizing the *Atg5$^{f/f}$;Aqp5-Cre* mouse model which harbors a conditional knockout of Atg5 in salivary acinar cells. At day 3 following a single 5 Gy dose of targeted head and neck radiation, male *Atg5$^{+/+}$;Aqp5-Cre* mice have a 12% reduction in salivary flow rates from unirradiated (UT), while salivary acinar autophagy-deficient *Atg5$^{f/f}$;Aqp5-Cre* mice exhibited ~45% reduction in flow rates from UT, which was significantly lower than irradiated *Atg5$^{+/+}$;Aqp5-Cre* mice (Figure 1A; $p < 0.05$). Female mice showed similar results at day 3 following radiotherapy: there was a 17% reduction in salivary output in *Atg5$^{+/+}$;Aqp5-Cre* mice, while *Atg5$^{f/f}$;Aqp5-Cre* autophagy-deficient mice displayed a 42% reduction in salivary flow rates, again significantly decreased from irradiated *Atg5$^{+/+}$;Aqp5-Cre* mice (Figure 1B). At day 14 following radiation, male *Atg5$^{+/+}$;Aqp5-Cre* mice showed a 17% reduction in salivary flow rates and *Atg5$^{f/f}$;Aqp5-Cre* autophagy-deficient mice exhibited a 40% reduction in salivary flow rates, which was significantly reduced from irradiated *Atg5$^{+/+}$;Aqp5-Cre* mice (Figure 1C). At day 14, a 19% reduction in salivary flow rates was detected in female *Atg5$^{+/+}$;Aqp5-Cre* mice, and *Atg5$^{f/f}$;Aqp5-Cre* salivary acinar-specific autophagy-deficient mice presented a 38% reduction (Figure 1D). At thirty days following radiation, while male *Atg5$^{+/+}$;Aqp5-Cre* mice regained part of salivary secretion, a persistent 41% reduction in salivary output was noted in *Atg5$^{f/f}$;Aqp5-Cre* autophagy-deficient mice (Figure 1E). On day 30 following treatment female *Atg5$^{+/+}$;Aqp5-Cre* mice have a 20% decrease and *Atg5$^{f/f}$;Aqp5-Cre* autophagy-deficient mice have a 38% decrease in salivary flow rates, significantly lowered from irradiated *Atg5$^{+/+}$;Aqp5-Cre* mice (Figure 1F; $p < 0.05$). We also determined whether radiation damage impacted the production and secretion of a key salivary protein, amylase. At day 30 following radiation *Atg5$^{f/f}$;Aqp5-Cre* autophagy-deficient mice display significantly decreased amylase area (~25% decrease from UT) within the acinar cells (Figure 1G) when compared to irradiated *Atg5$^{+/+}$;Aqp5-Cre* mice (~5% decrease from UT). These results were further confirmed through analysis of amylase secretion in saliva samples (Figure 1I). These results clearly demonstrate that both salivary flow rates and amylase protein production decreased significantly in male and female *Atg5$^{f/f}$;Aqp5-Cre* autophagy-deficient mice at chronic time points following radiation when compared to those in irradiated *Atg5$^{+/+}$;Aqp5-Cre* mice.

Targeted head and neck radiation does not robustly induce autophagy at early time points following treatment of wild-type mice. In order to understand the significant decrease in salivary gland function in autophagy-deficient mice, we evaluated the induction of autophagy in irradiated salivary glands from wild-type mice. Based on the understanding that there are no absolute markers for autophagy induction and some assays do not work in all tissues[33], a number of different analyses were conducted. Immunoblotting was performed with protein lysates collected from parotid glands of mice treated with a single 5 Gy dose of targeted head and neck radiation at respective time points. It has been previously demonstrated that apoptosis peaks at 24 hours post-radiation treatment, therefore we focused our analysis of autophagy induction from 4–8 hours following radiotherapy. A modest conversion of LC3-I to LC3-II was observed 8 hours post-radiation (Figure 2A, 2B); however there was no corresponding decrease in p62 levels (Figure 2A, 2E). Protein levels of Atg7 and Atg5 also remain unchanged 4 through 8 hours following radiation (Figure 2A–D). Structural evaluation of parotid glands from unirradiated and irradiated (8 hour) mice showed little evidence of autophagosome formation (Figure 2F). Quantification of the number of autophagosomes and lysosomes from irradiated tissues revealed 1.3/100 μm^2 and 1.7/100 μm^2, respectively which was very similar to unirradiated tissues. Localization of Atg5 and LC3 (Figure 2G–H) were also evaluated in tissue sections by immunohistochemistry. Atg5 appears to be ubiquitously expressed in acinar and ductal cells of the salivary gland and remains unchanged following radiation (Figure 2G). In addition, no differences in LC3 immunohistochemistry between untreated and irradiated tissues were observed (Figure 2H). Collectively, these data suggest there may only be a modest autophagy induction at early time points following radiation.

Pre-administration of IGF-1 to FVB mice induces autophagy at acute time points following targeted head and neck radiation. The salivary gland function of the autophagy-deficient mice was clearly decreased when compared to irradiated controls (Figure 1), yet surprisingly there was little evidence of robust autophagy induction in irradiated wild-type mice (Figure 2). Since both of these models have some level of radiation-induced loss of function, this led to the hypothesis that autophagy is induced in radiation models where there is a complete preservation of function. Previous studies have demonstrated that IGF-1 pretreatment decreased radiation-induced apoptosis and preserved salivary gland function[34]. In the current study, we examined if autophagy was a mechanism utilized by IGF-1 to allow for preservation of salivary gland function. In mice receiving IGF-1 prior to radiation, there is an increased conversion of LC3-I to LC3-II, elevated Atg7 and Atg5 and decreased p62 protein levels 6–8 hours following radiotherapy when compared to unirradiated tissues (Figure 3A–E; $p < 0.05$). The radiation-induced autophagy in parotid glands of IGF-1-pre-administrated mice was confirmed by increased autophagosome and lysosome detection through electron microscopy examination (Figure 3F). Quantification of the number of autophagosomes and lysosomes from tissues receiving IGF-1 prior to radiation revealed 2.4/100 μm^2 and 5.1/100 μm^2 respectively which was elevated over irradiated controls (Figure 3F). Similar to irradiated tissues, Atg5

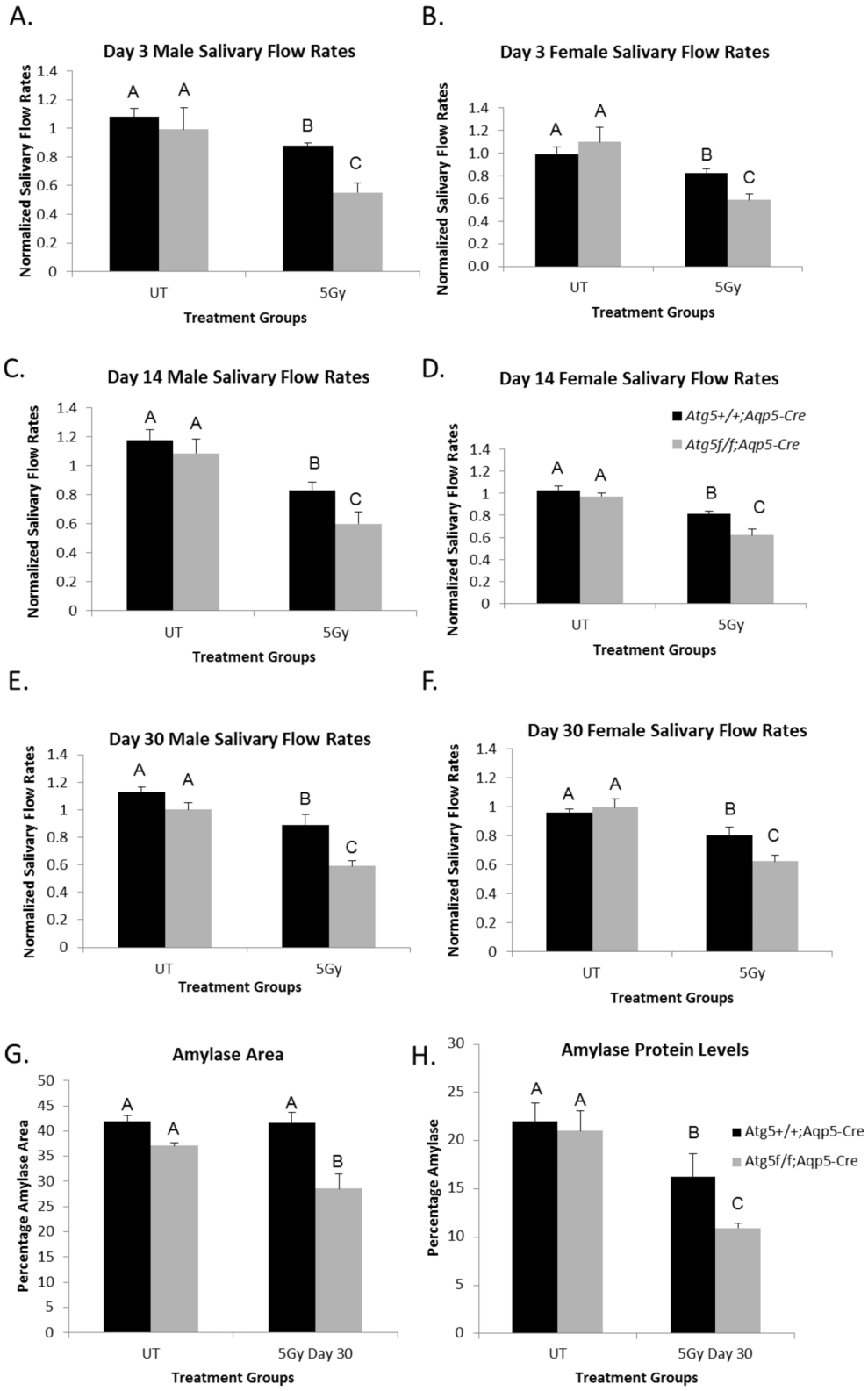

Figure 1 | Conditional knockout of *Atg5* in the salivary glands results in significantly decreased salivary flow rates and amylase production following targeted head and neck radiation. The head and neck region of male and female *Atg5*$^{+/+}$*;Aqp5-Cre* mice (black bar) and *Atg5*$^{f/f}$*;Aqp5-Cre* autophagy-deficient mice (gray bar) were exposed to a single 5 Gy radiation dose. UT: untreated/unirradiated. Data displayed as the mean ± SEM. Treatment groups with the same letters are not significantly different from each other. (A.–F.) Stimulated salivary flow rates were determined as described in Materials and Methods on days 3 (A.–B.), 14 (C.–D.) and 30 (E.–F.) following treatment. $p < 0.05$; n ≥ 15 per genotype. UT: untreated. (G.) Serial sections were stained to determine amylase area in parotid glands. The graph represents the positive amylase area as a percentage of the total parotid area. $p < 0.05$, n = 4 per genotype/per treatment. (H.) Stimulated saliva was collected from mice 30 days after treatment with a single 5 Gy dose of targeted head and neck radiation and analyzed for total protein content as described in Materials and Methods. The graph represents the percentage of amylase protein (ranging from 50–57 kD) $p < 0.05$, n = 10 per genotype/per treatment.

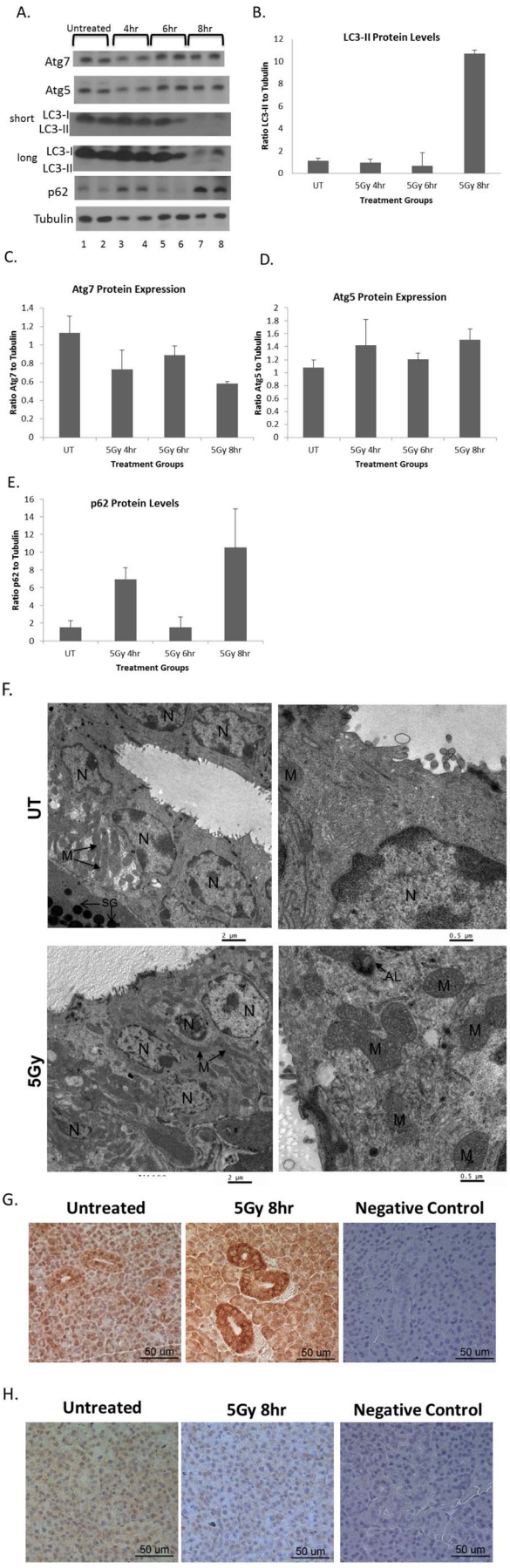

Figure 2 | Autophagy is not robustly induced at acute time points following targeted head and neck radiation. The head and neck region of female FVB wild-type mice were irradiated. Parotid tissue was collected at 4, 6, and 8, hours after treatment and representative duplicate samples are shown in each immunoblot. UT: untreated. Data displayed as the mean ± SEM. Treatment groups with the same letters are not significantly different from each other. (A.–E.) Protein lysates were prepared from parotid glands and Western blotting was performed as described in Materials and Methods. Tubulin was used to confirm equal loading. All gel images are cropped to display only the important bands for clarity. (A.) Parotid tissues were treated as stated above and collected at 4–8 hours following radiation for immunoblotting and prepared as described in the materials and methods, and membranes were probed for Atg7 (top panel), Atg5 (second panel), short LC3 exposure (third panel), long LC3 exposure (fourth panel) and p62 (fifth panel) with Tubulin (bottom panel) as a loading control. (B.) The graph represents the ratio of LC3-II to the loading control Tubulin, which was quantified using densitometry. n = 2 per time point/treatment. (C.) The graph represents the ratio of Atg7 to the loading control Tubulin, which was quantified using densitometry. $p < 0.05$, n = 3 per time point/treatment. (D.) The graph represents the ratio of Atg5 to the loading control Tubulin, which was quantified using densitometry. $p < 0.05$, n = 3 per time point/treatment. (E.) The graph represents the ratio of p62 to the loading control Tubulin, which was quantified using densitometry. n = 2 per time point/treatment. (F.) Representative electron microscopy images of parotid glands of untreated mice (*top panels*), mice at 8 hours post-radiation (*middle panels*). AL: autolysosome; AP: autophagosome; M: mitochondria; N: nucleus. (G.) Representative images of immunohistochemistry performed using an antibody against Atg5. (H.) Representative images of immunohistochemistry performed using an antibody against LC3.

appeared ubiquitously expressed across acinar and ductal cells of the salivary glands receiving IGF-1 prior to radiation (Figure 3G). In addition, salivary glands of mice treated with IGF-1 prior to radiation contained increased punctate LC3 staining (Figure 3H) when compared to unirradiated or irradiated mice. (Figure 3H compared to 2H). Taken together, these data suggest autophagy is induced when IGF-1 is administered prior to radiation.

Autophagy is required for preservation of salivary gland function in mice receiving IGF-1 prior to radiation. It has been previously shown that administration of IGF-1 prior to radiation completely prevents radiation-induced salivary gland dysfunction[34–36]. Based on the increase in autophagy markers (Figure 3), it was important to determine if autophagy was required for IGF-1-mediated preservation of salivary gland function. Administration of IGF-1 to autophagy-deficient mice (*Atg5$^{f/f}$;Aqp5-Cre*) failed to preserve salivary flow rates when compared to IGF-1 administration in *Atg5$^{+/+}$;Aqp5-Cre* mice at acute and chronic time points post-irradiation (Figures 4A–C). The loss of salivary gland function in irradiated *Atg5$^{f/f}$;Aqp5-Cre* autophagy-deficient mice receiving IGF-1 was similar to these same mice treated with radiation alone (Figure 1). Taken together, these data suggest autophagy is required for IGF1-mediated preservation of salivary gland function.

Salivary acinar autophagy-deficient Atg5$^{f/f}$;Aqp5-Cre mice exhibit significantly increased levels of apoptosis at 24 and 48 hours following targeted head and neck radiation. Apoptosis regulation has been shown to play a central role in the preservation of salivary gland function following radiation[15,17]. In addition, previous studies have shown that the conditional knockout of autophagy increases apoptotic cell death in both untreated and stressed conditions[19,37,38]. We aimed to determine if the observed changes in salivary secretion in *Atg5$^{f/f}$;Aqp5-Cre* autophagy-deficient mice (Figure 1) is

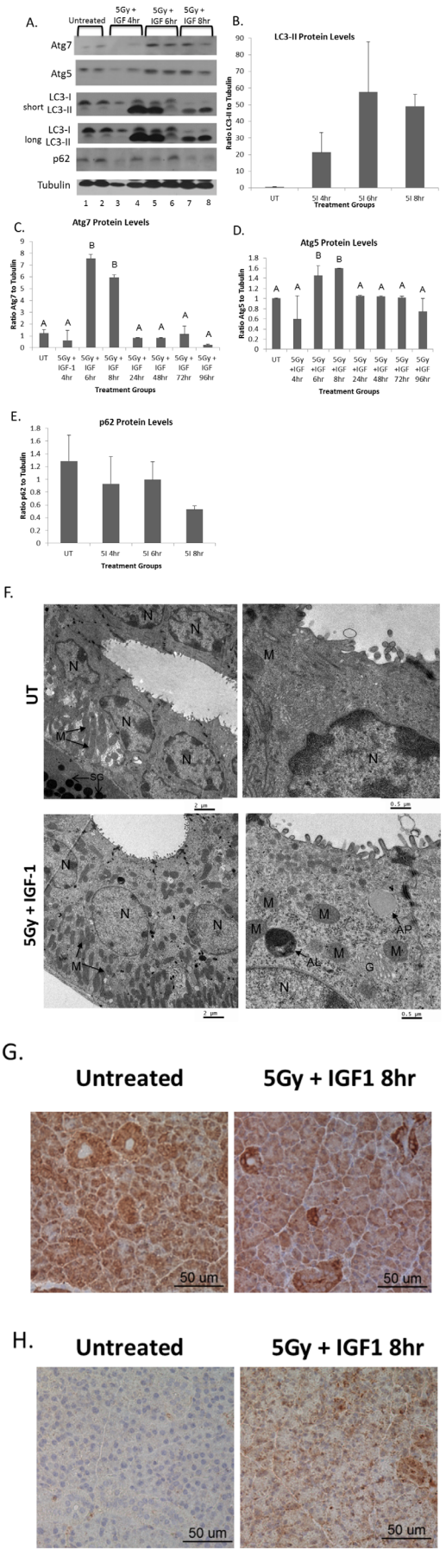

Figure 3 | Radiation with IGF-1 pretreatment increases autophagy 6–8 hours following treatment. (A.–I.) The head and neck region of female FVB wild-type mice were irradiated ± IGF-1 pretreatment. Parotid tissue was collected at 4, 6, and 8 hours after treatment and representative duplicate samples are shown in each immunoblot. UT: untreated. Data displayed as the mean ± SEM. Treatment groups with the same letters are not significantly different from each other within the same time point. (A.–E.) Protein lysates were prepared from parotid glands and western blotting was performed as described in Materials and Methods. Tubulin was used to confirm equal loading of lanes. All gel images are cropped to display only the important bands for clarity. (A.) Parotid tissues were treated as stated above and collected at 4–8 hours following radiation for immunoblotting and prepared as described in the materials and methods, and membranes were probed for Atg7 (top panel), Atg5 (second panel), short LC3 exposure (third panel), long LC3 exposure (fourth panel) and p62 (fifth panel) with Tubulin (bottom panel) as a loading control. (B.) The graph represents the ratio of LC3-II to the loading control Tubulin, which was quantified using densitometry. n = 2 per time point/treatment. (C.) The graph represents the ratio of Atg7 to the loading control Tubulin, which was quantified using densitometry. $p < 0.05$, n = 3 per time point/treatment. (D.) The graph represents the ratio of Atg5 to the loading control Tubulin, which was quantified using densitometry. $p < 0.05$, n = 3 per time point/treatment. (E.) The graph represents the ratio of p62 to the loading control Tubulin, which was quantified using densitometry. n = 2 per time point/treatment. (F.) Representative electron microscopy images of parotid glands of untreated mice (*top panels*) and mice pre-treated with IGF-1 at 8 hours post-radiation (*bottom panels*). AL: autolysosome; AP: autophagosome; M: mitochondria; N: nucleus. (G.) Representative images of immunohistochemistry performed using an antibody against Atg5. (H.) Representative images of immunohistochemistry was performed using an antibody against LC3.

accompanied with elevated apoptosis. *Atg5$^{f/f}$;Aqp5-Cre* autophagy-deficient mice exhibited a 16% increase in apoptosis of salivary acinar cells, measured via cleaved caspase-3 immunohistochemistry, from unirradiated mice at 24 hours following targeted head and neck radiation (Figure 5A–B). In contrast, radiation caused a 3.5% increase in apoptosis in *Atg5$^{+/+}$;Aqp5-Cre* mice. *Atg5$^{f/f}$;Aqp5-Cre* autophagy-deficient mice maintained elevated levels of apoptosis (~5%) at 48 hours following irradiation compared to a 2.5% increase detected in *Atg5$^{+/+}$;Aqp5-Cre* irradiated mice (Figure 5B). However, there was no significant change in apoptosis levels at 72 hours following radiation in both *Atg5$^{f/f}$;Aqp5-Cre* autophagy-deficient mice and *Atg5$^{+/+}$;Aqp5-Cre* mice (Figure 5B). Altogether, we conclude that the inactivation of autophagy in salivary acinar cells significantly increased the levels of apoptosis following irradiation.

An inverse correlation between autophagy and apoptosis in the parotid glands following targeted head and neck radiation. The exact interplay between apoptosis and autophagy remains elusive and it appears to be both tissue and stress context-dependent[17,18,20,30,39,40]. Based on the differences in autophagy (comparing Figures 2 and 3) and apoptosis induction[15,41,42] in irradiated mice ± IGF-1, we sought to define the interplay between autophagy and apoptosis in parotid glands. Previous studies have shown that increased apoptosis in salivary acinar cells begins at 8 hours following radiation, and peaks at 24 hours post-treatment; therefore we selected 4, 6 and 8 hour time points for early analysis of the interaction between these processes. At four hours post-radiation, there was a significant decrease in Beclin-1 protein levels, a known autophagy regulator, when compared to glands of unirradiated mice (Figure 6A, 6C). However, there was no change in Beclin-1 protein levels between unirradiated and irradiated mice at six and eight hours (Figures 6A, 6C). In contrast, there was a significant increase in

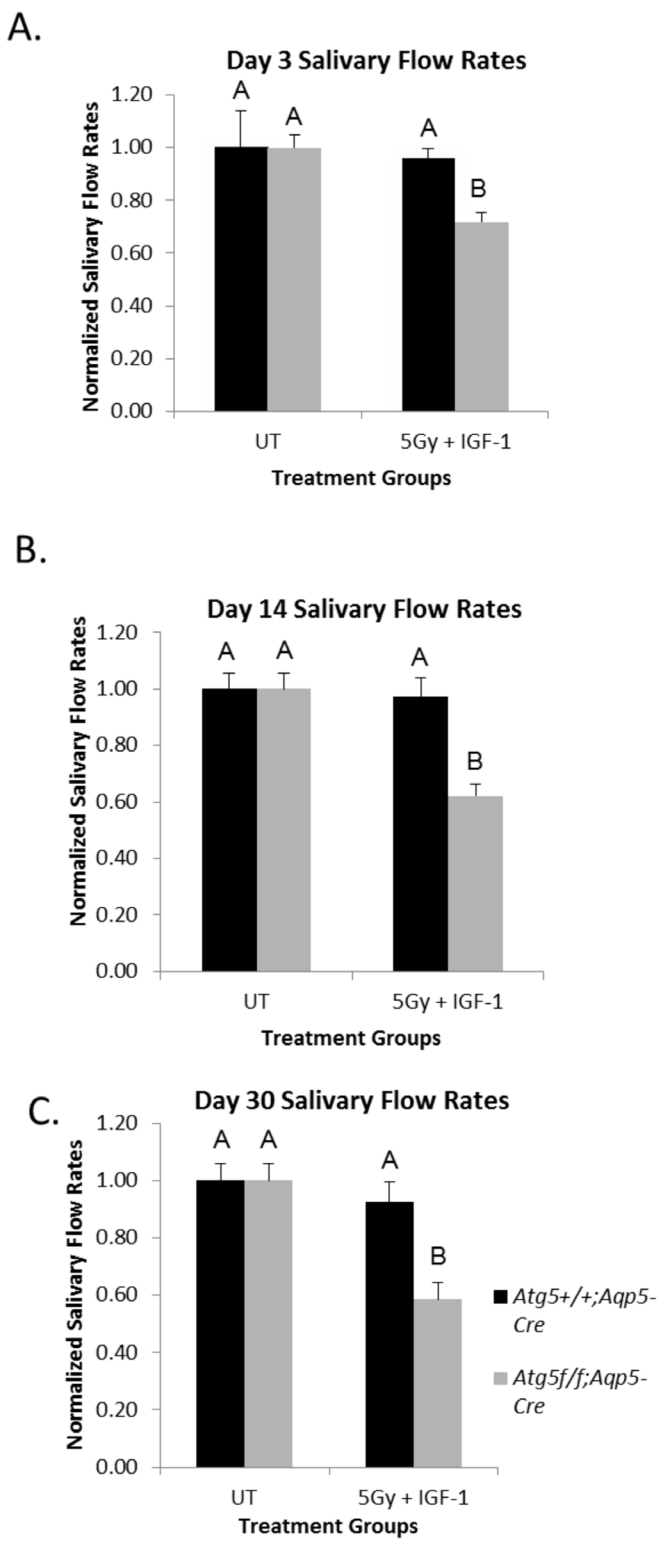

Figure 4 | IGF1 is unable to preserve salivary gland function in *Atg5$^{f/f}$;Aqp5-Cre*, autophagy-deficient mice. (A.–C.) The head and neck region of *Atg5$^{+/+}$;Aqp5-Cre* mice and *Atg5$^{f/f}$;Aqp5-Cre* autophagy-deficient mice were irradiated ± IGF-1 pretreatment. UT: untreated. Data displayed as the mean ± SEM. Treatment groups with the same letters are not significantly different from each other. Stimulated salivary flow rates were determined as described in Materials and Methods on days 3 (A.), 14[54], and 30 (C.) following treatment. $p < 0.05$; n ≥ 5 per genotype.

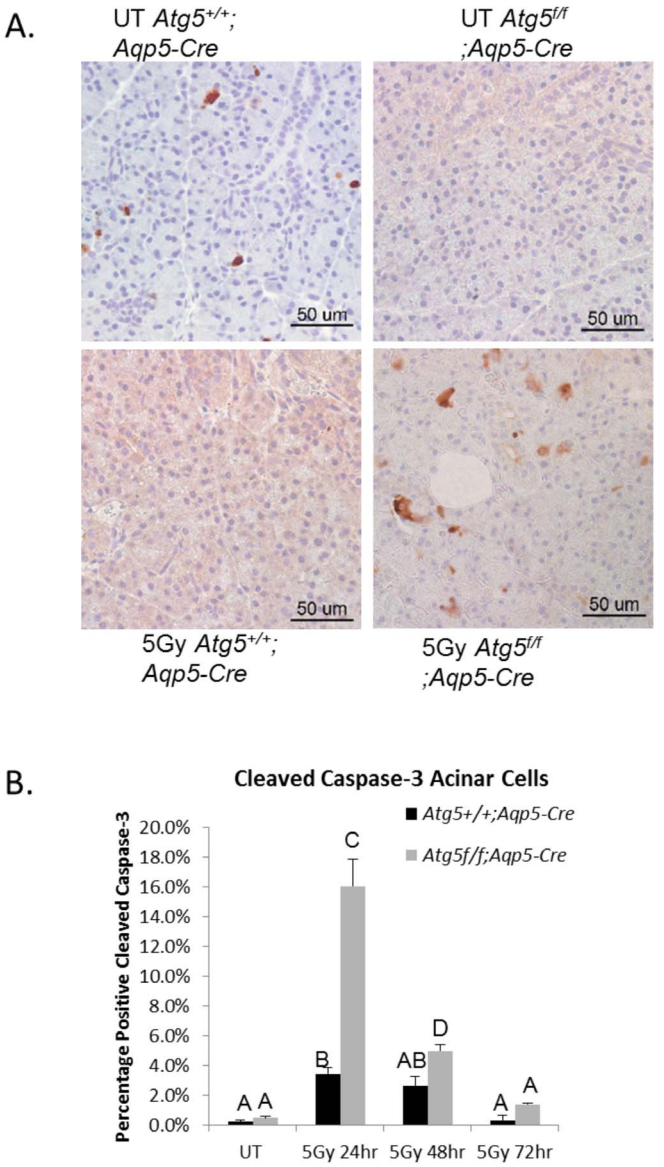

Figure 5 | *Atg5$^{f/f}$;Aqp5-Cre*, autophagy-deficient mice have significantly increased levels of apoptosis at 24 and 48 hours following targeted head and neck radiation. Salivary gland tissues were collected from both male and female *Atg5$^{+/+}$;Aqp5-Cre* and *Atg5$^{f/f}$;Aqp5-Cre* autophagy-deficient mice at 24, 48, and 72 hours following radiation treatment. Immunohistochemistry was performed using an antibody against cleaved caspase-3. UT: untreated. Treatment groups with the same letters are not significantly different from each other. (A.) Representative images of positive cleaved caspase-3 staining. (B.) The graph represents the number of acinar cells with positive cleaved caspase-3 staining as a percentage of the total number of acinar cells in the field of view. The data are displayed as the mean ± standard error of the mean of all data from 4–8 mice per group; $p < 0.05$.

Beclin-1 protein levels in glands of irradiated, IGF-1-pretreated mice at four, six, and eight hours (Figures 6B–C). Bcl-2, an anti-apoptotic protein, increased exclusively in the glands of irradiated mice at eight hours following treatment (Figures 6A, 6D). Interestingly, Bcl-2 was not significantly changed in the glands of irradiated mice treated receiving IGF-1 pretreatment (Figures 6B, 6D).

We then explored the relationship between Beclin-1 and Bcl-2 bound to Ambra1 by co-immunoprecipitation assays (Figure 6E–F). Previous studies have established that apoptotic cell death occurs

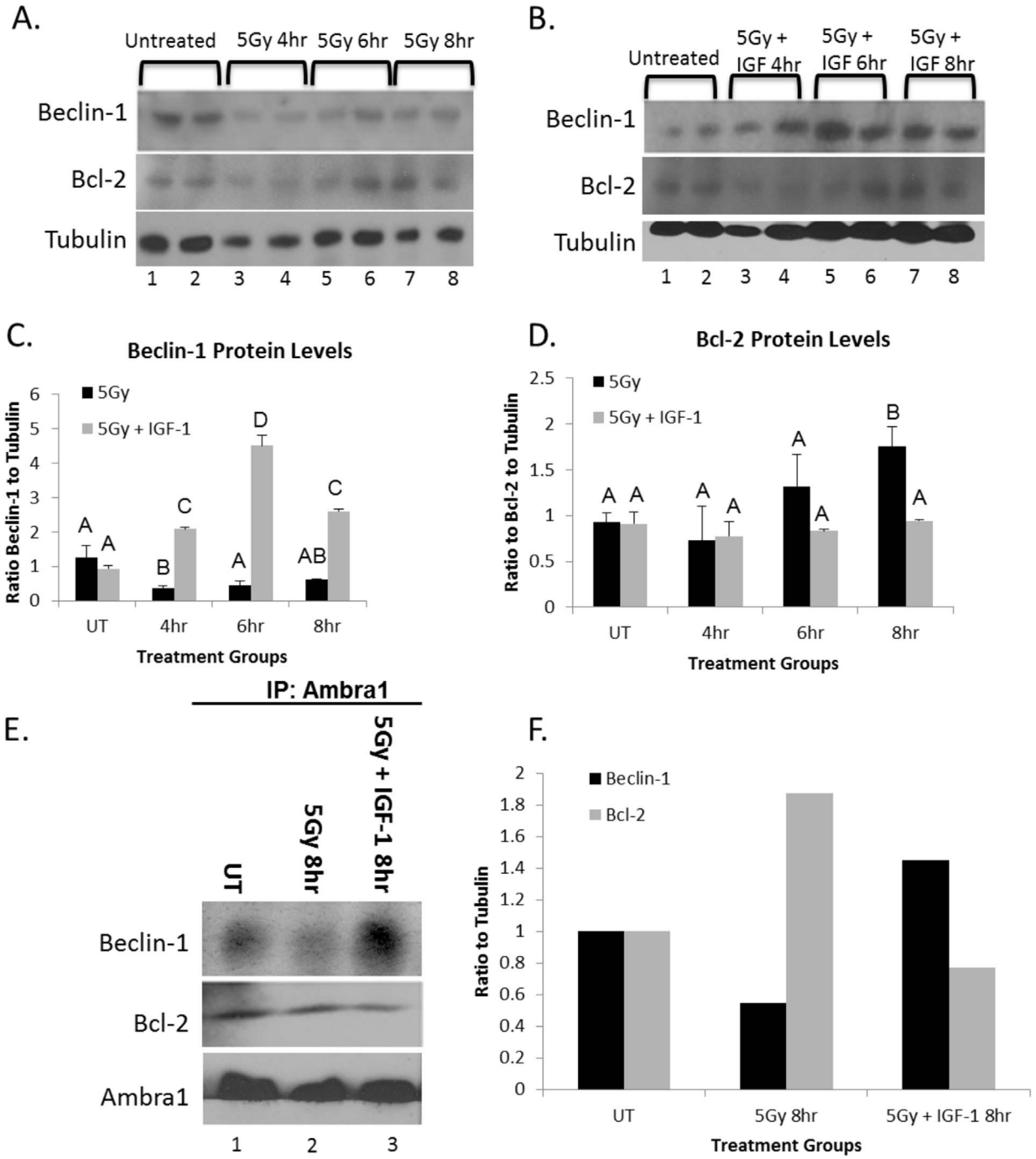

Figure 6 | Analysis of Ambra1, Beclin-1, and Bcl-2 show an inverse relationship between autophagy and apoptosis in the parotid glands following targeted head and neck radiation. (A.–D.) The head and neck region of female FVB wild-type mice were irradiated ± IGF-1 pretreatment. Protein lysates were prepared from parotid glands and western blotting was performed as described in Materials and Methods. Tubulin was used to confirm equal loading of lanes. All gel images are cropped to display only the important bands for clarity. $p < 0.05$; n = 3 per treatment group/time point. UT: untreated. Data displayed as the mean ± SEM. Treatment groups with the same letters are not significantly different from each other. (A.) Parotid tissues were treated as stated above and collected at 4–8 hours following radiation for immunoblotting and prepared as described in the materials and methods, and membranes were probed for Beclin-1 (top panel) and Bcl-2 (middle panel), with Tubulin (bottom panel) as a loading control. (B.) Parotid tissues were treated as stated above and collected at 4–8 hours following radiation for immunoblotting and prepared as described in the materials and methods, and membranes were probed for Beclin-1 (top panel) and Bcl-2 (middle panel), with Tubulin (bottom panel) as a loading control. (C.) The graph represents the ratio of Beclin-1 to the loading control Tubulin, which was quantified using densitometry. (D.) The graph represents the ratio of Bcl-2 to the loading control Tubulin, which was quantified using densitometry. (E.) Protein lysates were prepared from parotid glands immunoprecipitated with Ambra1 antibody as described in the materials and methods. Immunoblotting was performed to detect Ambra1 bound to Beclin-1 or Bcl-2. (F.) The graph represents the ratio of Beclin-1 or Bcl-2 to Ambra1, which was quantified from (E.) using densitometry.

and autophagy is inhibited when Ambra1 is bound to Bcl-2, and the autophagic process proceeds and apoptosis is inhibited when Ambra1 is bound to Beclin-1[17,20]. Consistently, we observed increased levels of Bcl-2 bound to Ambra1 in parotid glands of irradiated mice when compared to parotid glands from untreated or irradiated mice receiving IGF-1 pretreatment (Figures 6E–F). Conversely, increased Beclin-1 bound to Ambra1 was detected in glands of irradiated mice that were pre-administrated with IGF-1 (Figures 6E–F). Taken together, we postulate that IGF-1 pretreatment facilitated a switch of Ambra-1 association with Bcl-2 to an association with Beclin-1 in parotid glands of irradiated mice.

Discussion

It is well-established that radiotherapy for head and neck cancer diminishes salivary gland function and greatly decreases the quality of life for these patients. The purpose of this study was to evaluate the role of autophagy in the salivary gland response to targeted head and neck radiation. We found that 1) autophagy-deficient *Atg5$^{f/f}$;Aqp5-Cre* mice have increased radiosensitivity; 2) IGF-1 treatment prior to radiation increases autophagosome formation at 4–8 hours following radiotherapy; 3) IGF-1 pretreatment does not preserve salivary gland function in autophagy-deficient *Atg5$^{f/f}$;Aqp5-Cre* mice; and 4) there is an inverse correlation between autophagy and apoptosis in the salivary glands following radiation.

The conditional knockout model of *Atg5*, *Atg5$^{f/f}$;Aqp5-Cre*, in the acinar cells of salivary glands exhibited a significant decrease in stimulated salivary flow rates following a single 5 Gy dose of targeted head and neck radiation in both males and females when compared to those in irradiated *Atg5$^{+/+}$;Aqp5-Cre* mice at days 3, 14, and 30 (Figures 1A–F). Our results are similar to other studies using knockdown models of autophagy which have reported that loss of autophagy capacity leads to increased DNA damage, cell death and dysregulation of the cell cycle following treatment with cytotoxic agents or radiation[39,43].

Atg5$^{f/f}$;Aqp5-Cre autophagy-deficient mice also display increased rates of apoptosis at 24 and 48 hours following targeted head and neck radiation when compared to irradiated *Atg5$^{+/+}$;Aqp5-Cre* mice (Figure 5). The loss of salivary secretory function is most likely due to significantly increased rates of apoptosis, analogous to other models of radiation-induced salivary gland dysfunction[15,36]. However, these results could also be due to an alteration of the GPCRs or ion channels following radiation. A recent study by Liu et al found that radiation leads to activation of the calcium-permeable channel, transient potential melastatin-like 2 (TRPM2), in the salivary glands and loss of TRPM2 is protective against radiation-induced salivary gland dysfunction[44]. Unfortunately, no other studies have been conducted into the role of either GPCRs or ion channels in autophagy and salivary gland tissue following radiation, suggesting that considerably more work in this area is needed and is an interesting future direction.

We demonstrated here that mice treated with radiation plus IGF-1 pretreatment result in accelerated autophagosome formation, presumably leading to autophagy induction at earlier time points (6–8 hours) post-irradiation (Figures 3A–H). We have previously shown that mice treated with radiation plus IGF-1 pretreatment have preserved salivary gland function via decreased apoptosis and cell cycle arrest[15,36]; therefore we speculate that the increase in autophagy could be a beneficial mechanism involved in this model. Indeed, IGF-1 pretreatment could not preserve salivary gland function in *Atg5$^{f/f}$;Aqp5-Cre* autophagy-deficient mice when compared to *Atg5$^{+/+}$;Aqp5-Cre* mice under the same treatment (Figure 4). Initially, these results seem counterintuitive as IGF-1 activates the PI3K/Akt/mTOR pathway in unstressed conditions, which would inhibit autophagy and increase proliferation. However, a previous study by Mitchell *et al* found that following damage (radiation) of normal tissues, IGF-1 pretreatment induces cell cycle arrest and allows for cellular repair to occur[45]. In addition, Lee *et al* have previously described a link between cell cycle regulation and autophagy under conditions of nutrient starvation[46]. In this model, autophagy deficient MEFs (Atg7−/−) were unable to induce p21 expression and exit the cell cycle three hours into the starvation treatment. Conceivably, induction of autophagy and cell cycle arrest may be linked and both of these processes could equally contribute to the preservation of salivary secretory function in irradiated mice receiving IGF-1 pretreatment. Furthermore, one study found that increased IGF-1 expression in the skeletal muscle, through resistance exercise training, led to decreased phosphorylation of both Akt and mTOR while increasing autophagy regulatory proteins[47]. We hypothesize that IGF-1 may activate different signaling pathways under stressed conditions, such as that following radiotherapy or exercise, than in a normal tissue environment.

It is well established that there is signaling crosstalk between apoptosis and autophagy; however, the exact interplay between these two cellular mechanisms remains elusive[19,39,48]. It has been previously shown that autophagy can inhibit apoptosis during cellular starvation via the breakdown of cellular components to provide metabolites and maintain ATP levels[49]. Paradoxically, studies also reported that autophagy can contribute to apoptosis. For example, Martin et al found that autophagy precedes apoptosis during developmental degradation of salivary glands of *D. melanogaster*[50,51]. The interplay between apoptosis and autophagy in irradiated salivary glands was determined through the evaluation of Beclin-1 or Bcl-2 binding to Ambra1. The inverse correlation between binding of Bcl-2 or Beclin-1 to Ambra1 has been utilized in previous studies to reflect the antagonistic roles of these cellular mechanisms[17–20]. It has been suggested that increased binding of Beclin-1 to Ambra-1 signals autophagy and elevated binding of Bcl-2 and Ambra1 sequesters both these proteins leading to an induction of apoptosis. In irradiated parotid glands, there was decreased binding of Beclin-1 to Ambra1 (Figure 6F), consistent with the lack of autophagy induction in this treatment group (Figures 2A–H). Moreover, there was an increase in Bcl-2 bound to Ambra1 in these tissues (Figure 6F), presumably promoting the sequestration of Bcl-2[27,45,47] and thereby leading to an induction of apoptosis which has been reported in salivary acinar cells[15,20,23,36,49,50,52,53]. In contrast, mice treated with radiation plus IGF-1 pretreatment have increased levels of Beclin-1 bound to Ambra1 (Figure 6F) leading to preserved salivary function through autophagy induction (Figures 3A–H).

In conclusion, we show here that autophagy may be playing a beneficial role in the salivary glands following targeted head and neck radiation through both the increased radiosensitivity of *Atg5$^{f/f}$;Aqp5-Cre* autophagy-deficient mice and increased levels of autophagy in a radiation protection model (pretreatment with IGF-1). Our results suggest that autophagy and apoptosis have an inverse relationship in parotid glands following targeted head and neck radiation and imply that autophagy and apoptosis may have an inhibitory effect on one another. These findings are significant as autophagy inducers could be utilized in the clinical setting to preserve salivary gland function in head and neck cancer patients. Importantly, the use of pharmacological interventions to induce autophagy to preserve normal tissue function would need to be balanced against the therapeutic response of the primary tumor as autophagy has been shown to be a tumor resistance mechanism[51]. The preservation of salivary gland function would ameliorate the multitude of maladies associated with radiation-induced salivary gland dysfunction and greatly improve quality of life.

1. Denaro, N., Numico, G., Pazzaia, T., Vitiello, R. & Merlano, M. C. The role of neck dissection after radical chemoradiation for locally advanced head and neck cancer: should we move back? *Oncology* **84**, 174–185 (2013).
2. Grundmann, O., Mitchell, G. & Limesand, K. H. Sensitvity of Salivary Glands to Radiation: from Animal Models to Therapies. *J Dent Res* **88**, 894–903 (2009).

3. Vissink, A. *et al.* Clinical management of salivary gland hypofunction and xerostomia in head-and-neck cancer patients: successes and barriers. *Int J Radiat Oncol Biol Phys* **78**, 983–991 (2010).
4. Maiuri, C. M., Zalckvar, E., Kimchi, A. & Kroemer, G. Self-eating and self-killing: crosstalk between autophagy and apoptosis. *Nat Rev Mol Cel Biol* **8**, 741–752 (2007).
5. Wirawan, E., Lippens, S., Agostinis, P. & Vandenabeele, P. Autophagy: for better of for worse. *Cell Res* **22**, 43–61 (2012).
6. Amaravadi, R. K. *et al.* Autophagy inhibition enhances therapy- induced apoptosis in a Myc-induced model of lymphpoma. *J Clin Inves* **117**, 326–336 (2007).
7. Chen, S. *et al.* Autophagy is a therapeutic target in anticancer drug resistance. *Biochim and Biophys Acta* **1806**, 220–229 (2010).
8. Choi, A. M. K. & Levine, B. Autophagy in human health and disease. *NEJM* **368**, 651–662 (2013).
9. Hoyer-Hansen, M. Autophagy: an emerging target for cancer therapy. *Autophagy* **4**, 574–580 (2008).
10. Kim, K. W. *et al.* Autophagy for cancer therapy through inhibition of proapoptotic proteins and mTOR signaling. *J Biol Chem* **281**, 36883–36890 (2006).
11. Mathew, R. & White, E. Role of autophagy in cancer. *Nat Rev* **7**, 961–967 (2007).
12. Palumbo, S. Autophagy and ionizing radiation in tumors: the "survive or not survive" dilemma. *J of Cell Phys* **228**, 1–8 (2013).
13. Wang, T. *et al.* Effect of ionizing radiation on acinar morphogenesis of human prostatic epithelial cells under three-dimensional culture conditions. *Neoplasma* **59**, 269–281 (2012).
14. Moretti, L., Kim, K. W. & Lu, B. Crosstalk between Bak/Bax and mTOR signaling regulates radiation-induced autophagy. *Autophagy* **3**, 142–144 (2007).
15. Avila, J. L., Grundmann, O., Burd, R. & Limesand, K. H. Radiation-induced salivary gland dysfunction results from p53-dependent apoptosis. *Int J Radiat Oncol Biol Phys* **73**, 523–529 (2009).
16. Mitchell, G. *et al.* IGF1 activates cell cycle arrest following irradiation by reducing binding of deltaNp63 to the p21promoter. *Cell Death Dis* **10**, e50 (2010).
17. Fimia, G. M. *et al.* Ambra1 regulates autophagy and development of the nervous system. *Nat* **447**, 1121–1125 (2007).
18. Codogno, P. Atg5: more than an autophagy factor. *Nat Cell Biol* **8**, 1045–1047 (2006).
19. Fimia, G. M. Regulation of autophagy in mammals and its interplay with apoptosis. *Cell Mol Life Sci* **67**, 1581–1588 (2010).
20. Funderburk, S. F. & Yue, Z. The Beclin 1-VPS34 complex - at the crossroads of autophagy and beyond. *Trends in Cell Biology* **20**, 355–362 (2010).
21. Klionsky, D. Autophagy: from phenomenology to molecular understanding in less than a decade. *Nat Rev* **8**, 931–937 (2007).
22. Morgan-Bathke, M. *et al.* Deletion of Atg5 shows a role of autophagy in salivary homeostatic control. *J of Dent Res* **92**, 911–917 (2013).
23. Nielsen, S., Christensen, B. M. & Agre, P. Aquaporins in complex tissues. II. Subcellular distribution in respiratory and glandular tissues of rat. *Am J Physiol* **273**, C1549–C1561 (1997).
24. Azlina, A. *et al.* Roles of lysosomal proteolytic systems in AQP5 degradation in the submandibular gland of rats following chorda tympani parasympathetic denervation. *Am J Physiol Gastrointest Liver Physiol* **299**, G1106–1117 (2010).
25. Lin, A. L. *et al.* Measuring short-term gamma-irradiation effects on mouse salivary gland function using a new saliva collection device. *Archives of Oral Biology* **46**, 1085–1089 (2001).
26. Ferreira, T. *ImageJ User Guide* (NIH 2012).
27. Nutting, C. *et al.* Parotid-sparing intensity modulated versus conventional radiotherapy in head and neck cancer (PARSPORT): a phase 3 multicentre randomised controlled trial. *Lancet Oncol* **12**, 127–136 (2011).
28. Lin, H. H. *et al.* Identification of AAA ATPase VPS4B-dependent pathway that modulates epidermal growth factor receptor abundance and signaling during hypoxia. *Mol Cell Biol* **32**, 1124–1138 (2012).
29. Grundmann, O., Mitchell, G. & Limesand, K. H. Sensitivity of Salivary Glands to Radiation: from Animal Models to Therapies. *J Dent Res* **88**, 894–903 (2009).
30. Kim, K. W. *et al.* Autophagy upregulation by inhibitors of caspase-3 and mTOR enhances radiotherapy in a mouse model of lung cancer. *Autophagy* **4**, 659–668 (2008).
31. Wang, Y. *et al.* Decrease of autophagy activity promotes malignant progression of tongue squamous cell carcinoma. *Oral Pathology and Medicine* **ePub**, 1–8 (2013).
32. Djavaheri-Mergny, M. NF-KB activation represses tumor necrosis factor-alpha-induced autophagy. *J Biol Chem* **281**, 30373–30382 (2006).
33. Klionsky, D. J. *et al.* Guidelines for the use and interpretation of assays for monitoring autophagy. *Autophagy* **8**, 445–544 (2012).
34. Limesand, K. H. *et al.* Insulin-Like Growth Factor-1 Preserves Salivary Gland Function After Fractionated Radiation. *Int J Radiation Oncology Biol Phys* **78**, 1–8 (2010).
35. Limesand, K. H. & Anderson, S. M. Suppression of radiation-induced salivary gland dysfunction by IGF-1. *PLoS.ONE.* **4**, e4663 (2009).
36. Limesand, K. H. & Anderson, S. M. Suppression of radiation-induced salivary gland dysfunction by IGF-1. *PLoS One* **4**, e4663 (2009).
37. Shen, S. *et al.* Association and dissociation of autophagy, apoptosis, and necrosis by systematic chemical study. *Oncogene* **30**, 4544–4556 (2011).
38. Aburto, M. R. *et al.* Early otic development depends on autophagy for apoptotic cell clearance and neural differentiation. *Cell Death and Disease* **3**, e394 (2012).
39. Levine, B. p53: The Janus of autophagy? *Nat Cell Biol* **10**, 637–639 (2008).
40. Mauiri, M. C., Mimchi, A. & Kroemer, G. Self-eating and self-killing: crosstalk between autophagy and apoptosis. *Nat Rev Mol Cell Biol* **8**, 741–752 (2007).
41. Limesand, K. H. & Anderson, S. M. MDM2 is required for suppression of apoptosis by activated Akt1 in salivary acinar cells. *Mol Cell Biol* **25**, 8840–8856 (2006).
42. Limesand, K. H. *et al.* Characterization of rat parotid and submandibular acinar cell apoptosis in primary culture. *In Vitro Cell Dev Biol Anim* **39**, 170–177 (2003).
43. Bae, H. Suppression of autophagy by FIP200 deletion impairs DNA damage repair and increases cell death upon treatments with anticancer agents. *Mol Cancer Res* **9**, 1232–1241 (2011).
44. Liu, X. *et al.* Loss of TRPM2 function protects against irradiation-induced salivary gland dysfunction. *Nat Comm* **4**, 1515 (2013).
45. Mitchell, G. C. *et al.* IGF1 activates cell cycle arrest following irradiation by reducing binding of deltaNp63 to the p21 promoter. *Cell Death Dis* **1**, e50 (2010).
46. Lee, I. H. *et al.* Atg7 modulates p53 activity to regulate cell cycle and survival during metabolic stress. *Science* **336**, 225–228 (2012).
47. Luo, L. *et al.* Chronic resistance training activates autophagy and reduces apoptosis of muscle cells by modulating IGF-1 and its receptors, Akt/mTOR and Akt/FOXO3a signaling in aged rats. *Experimental Gerontology* **48**, 427–436 (2013).
48. Djavaheri-Mergny, M. & Kroemer, G. Cross talk between apoptosis and autophagy by caspase-mediated cleavage of Beclin-1. *Oncogene* **29**, 1717–1719 (2010).
49. Lum, J. J. & Kong, M. Growth factor regulation of autophagy and cell survival in the absence of apoptosis. *Cell* **120**, 237–248 (2005).
50. Martin, D. N. Caspases function in autophagic programmed cell death in Drosophila. *Development* **131**, 275–284 (2004).
51. Berry, D. L. Growth arrest and autophagy are required for salivary gland degradation in Drosophila. *Cell* **131**, 1137–1148 (2007).
52. Luo, S. Apoptosis blocks Beclin 1-dependent autophagosome synthesis - an effect rescued by Bcl-xL. *Cell Death and Differentiation* **17**, 268–277 (2010).
53. Molejan, M. I. *et al.* The VMP1-Beclin-1 interaction regulates autophagy induction. *Sci. Rep.* **3**, 1055–1070 (2012).
54. Mizushima, N. *et al.* Autophagy fights disease through cellular self-digestion. *Nature* **451**, 1069–1075 (2008).

Acknowledgments

We would like to acknowledge Dr. Noboru Mizushima for kindly providing the *Atg5$^{f/f}$* mice. This work was supported in part by the National Institute of Health Research Grants R01DE10742, R01DE14183 (to D.K.A.), R01DE018888 (to K.H.L.) and RC1DE20335 (to D.K.A. and K.H.L.).

Author contributions

M.M.B., K.H.L. and D.K.A. wrote the main manuscript text. A.M.C. helped to prepare all of the figures for publication and prepared figure 1H. D.K.A. and H.H.L. prepared figures 2F and 3F. Z.I.H. prepared figures 2G–H and 3G–H. G.A.H. prepared figure 1A–F and figure 4. R.R.K. analyzed IHC images for publication. M.M.B. prepared figure 1G, figure 2A–E, figure 3A–E, figure 5 and figure 6. R.B. provided guidance for experimental design. All authors reviewed the manuscript.

Additional information

Supplementary information accompanies this paper at http://www.nature.com/scientificreports

Competing financial interests: The authors declare no competing financial interests.

How to cite this article: Morgan-Bathke, M. *et al.* Autophagy Correlates with Maintenance of Salivary Gland Function Following Radiation. *Sci. Rep.* **4**, 5206; DOI:10.1038/srep05206 (2014).